Int. J. Electrochem. Sci., 12 **(2017)** 5646 – 5656, doi: 10.20964/2017.06.60

International Journal of
ELECTROCHEMICAL
SCIENCE
www.electrochemsci.org

$CoWO_4$ Nanoparticles Prepared in Different Solvents and Their Pseudocapacitant Performances

Aiping Li, Yin Tu, Yue Zhu, Denghao Li, Wei Zhou, Xiufang Zhu, Liangdong Feng[*]

Jiangsu Provincial Engineering Laboratory for Salt Chemical Industry and New Materials, Huaian 223003, PR China; Department of Chemical Engineering, Huaiyin Institute of Technology, Huaian 223003, PR China
Jiangsu Provincial Key Laboratory for Interventional Medical Devices, Huaian 223003, PR China
[*]Email: ldfeng@hyit.edu.cn

Received: 12 March 2017 / *Accepted:* 24 April 2017 / *Published:* 12 May 2017

Cobalt tungstates ($CoWO_4$) nanoparticles have been successfully fabricated through a facile hydrothermal route by employing different solvents. The structure, morphology, surface area and pore distribution of the as-prepared products were characterized and their capacitances were investigated. The results showed that $CoWO_4$ nanoparticles synthesized in the mixed solvent of deionized water and ethylene glycol presented the highest specific capacitances of 1 817.14 $F \cdot g^{-1}$ at the discharge current density of 1.0 $A \cdot g^{-1}$. The high surface area and proper pore distribution contributed to this high specific capacitances. In addition, the $CoWO_4$ also showed good cycle-life stability.

Keywords: $CoWO_4$ nanoparticles, solvent, surface area, pore distribution, pseudocapacitance

1. INTRODUCTION

As one of the most important electrochemical energy storage systems, supercapacitors, also called electrochemical capacitors (ECs), have been attracted considerable research interest due to their high power density, long lifespan, and fast charge/discharge process [1-6]. Based on charge storage mechanisms and active materials utilized, supercapacitors can be classified into two types: electric double layer capacitors (EDLCs) and pseudocapacitors[7-9]. In general, pseudocapacitors, often based on transition metal oxides/hydroxides and conducting polymers, can provide high specific capacitance (SC) that is often several times higher than that of EDLCs due to higher levels of charge storage from redox reactions [10-12]. Recently, transition metal oxides or hydroxides have been extensively

investigated as pseudocapacitive materials, mainly ascribed to their storing charges via an electrical double layer mechanism, but also undergoing fast and reversible surface redox reactions.

Although in recent years, a lot of progress has been made with the development of pseudocapacitors, the main challenges are still the low energy density and poor overall performance, which have to be overcome in order to widen its applications. The pseudocapacitant properties of electrode materials can be greatly influenced by their structure including morphology, size, specific surface area, pore size and distribution [6]. For example, the porosity relevant to the development of high capacity is itself not a simple parameter, involving both pore sizes and pore-size distribution for a given overall specific area of the material. According to Lu *et al.*, the size, geometry, length, alignment of pores and the degree of pore ordering will all influence the performance of supercapacitors [13]. Therefore, the capacity strongly depends on the surface area of the electrode accessible to the electrolyte. However, very little work has yet been done in systematically studying the principles for optimizing electrode architectures, especially those involving the effecting of pore size on the pseudocapacitant properties of electrode materials.

As reported in some literatures, cobalt tungstates, an important material of ABO_4-type ternary metal oxides, have aroused much interest due to their low cost, abundant resources, environmental friendliness, excellent catalytic and electrochemical characteristics [14,15]. In addition, the binary metal oxides of tungstate present the conductivity on the order of 10^{-7}–10^{-3} $S \cdot cm^{-1}$, because the incorporation of W atoms can greatly enhance their conductivity in comparison with pure metal oxide [16]. Thus, $CoWO_4$ is predicted to be a very promising electrode material for pseudocapacitor materials. For example, Xing *et al.* prepared amorphous $CoWO_4$-amorphous and crystal $CoWO_4$-crystalline nanoparticles through simple wet-chemical and hydrothermal approaches, and proved that the amorphous structure, small size and narrow particle size distribution contributed to the high electrochemical performances of $CoWO_4$ [17]. Xu *et al.* prepared $CoWO_4$, $NiWO_4$ and $CoWO_4$@$NiWO_4$ nanocomposites by a facile chemical co-precipitation method and compared their supercapacitive performances [18]. Ye's group synthesized reduced graphene oxide-cobalt tungstate nanocomposites with enhanced electrochemical performances for supercapacitors using facile one-pot hydrothermal method, and attributed the good electrochemical performance of the nanocomposites to the increased electrical conductivity and the creation of new active sites due to the synergetic effect of reduced graphene oxide and $CoWO_4$ nanospheres [19]. Combining the good rate capability of $CoWO_4$ and the high specific capacity of $NiWO_4$, Wang *et al.* synthesized a series of mesoporous $NiWO_4$-$CoWO_4$ nanocomposite by a chemical co-precipitation method, the nanocomposite could reach a maximum specific capacity of 196.7 $C \cdot g^{-1}$ at 0.5 $A \cdot g^{-1}$ and retained 68% of the initial capacity when the discharging rate increased for 20 times [20]. By microwave irradiation method, Karuppuchamy's group obtained Co-WO_3 and $CoWO_4$, and the specific capacitance value for Co-WO_3 was only 45 $F \cdot g^{-1}$ at 0.25 $A \cdot g^{-1}$ [21]. Although applications of $CoWO_4$ have appeared in the energy storage field, the studies on $CoWO_4$ directly as electrode materials for supercapacitors are still less explored, and the investigations on the correlation between the pore size distribution and the capacitance performance of $CoWO_4$ are rarer.

Herein, we describe a facile hydrothermal preparation of $CoWO_4$ nanoparticles in different solvents and investigate their electrochemical performance as electrode materials. The resulting

products were characterized in detail using X-ray diffraction (XRD), scanning electron microscopy (SEM) and Brunauer-Emmett-Teller (BET) techniques. The pseudocapacitive performance of the material was also investigated by cyclic voltammetry (CV), chronopotentiometry (CP) and electrochemical impedance spectroscopy (EIS) measurements.

2. EXPERIMENTAL

2.1. Materials preparation

Analytical grade of cobalt chloride hexahydrate ($CoCl_2 \cdot 6H_2O$), sodium tungstate dihydrste ($Na_2WO_4 \cdot 2H_2O$), ethanol (CH_3CH_2OH, Et), ethylene glycol ($(CH_2OH)_2$, Eg) and potassium hydroxide (KOH) were purchased from Shanghai Chemical Reagent Co. All reagents were used without further purification, and deionized (DI) water was used throughout.

$CoWO_4$ nanoparticles were prepared through hydrothermal route. Firstly, 0.2 mmol $Na_2WO_4 \cdot 2H_2O$ were added into 40 ml DI water or DI water-Et or DI water-Eg or DI wate -Et-EG mixed solvent with vigorous stirring at room temperature to form a transparent solution, the volume ratio of mixed solvents were kept at 1:1 all through. Then, 0.2 mmol $CoCl_2 \cdot 6H_2O$ were dissolved in the above solution and stirring for 0.5 hours. The solutions were placed in 80 mL Teflon-sealed autoclaves and maintained at 150 °C for different times. The resulting products were washed with DI water and ethanol for several times, respectively, and dried at 80 °C for 24 hours.

2.2. Characterization

The crystallinity of the products were analyzed by a Bruker D8 Advance X-ray diffractometer at a scanning rate of 4°/min using Cu Kα radiation (λ = 0.15406 nm). The SEM images were carried out on a Quanta 250 FENG field-emission scanning electron microscopy (FESEM, FEI) with Energy dispersive spectrometry (EDS, Oxford UK). Multipoint nitrogen adsorption/desorption curves were recorded on an automatic Micromeritics Tristar II 3020 analyzer using Brunauer-Emmett-Teller (BET) gas adsorption method at 77 K. All samples were out-gassed at 100 ºC for 6 h under flowing nitrogen before measurements. The specific surface area values were calculated using the software of the instrument based on BET equation. Pore size and pore size distribution plots were obtained by Barrett–Joyner–Halenda (BJH) method using the cylindrical pore model [22].

Electrochemical experiments were carried out on a CHI 660C electrochemical workstation (Chenhua, Shanghai, China) at room temperature. A traditional three electrode configuration was used with $CoWO_4$ coated nickel foam sheet as the working electrode, a platinum foil (1×2 cm^2) and HgO/Hg (1.0 $mol \cdot L^{-1}$ KOH) served as counter electrode and reference electrode, respectively. The working electrodes were prepared by mixing the obtained $CoWO_4$ with 10 *wt*% polytetrafluoroethylene and 15 *wt*% acetylene black of the total electrode mass. A small amount of ethanol was added to this composite to make a more homogenous mixture, which was pressed on

nickel foam sheet, and vacuum-dried at 80 ˚C for 12 h. All potentials given below were relative to the HgO/Hg.

The electrochemical performance was characterized by cyclic voltammetry (CV), chronopotentiometry (CP) and electrochemical impedance spectroscopy (EIS) tests. The CV, CP and EIS studies were performed in a 6.0 mol·L^{-1} KOH deoxygenated aqueous. The electrochemical impedance spectra were measured by imposing a sinusoidal alternating voltage frequency of 1×10^{-2} to 1×10^{5} Hz with amplitude of 5 mV at open circuit potentials.

3. RESULTS AND DISCUSSION

The XRD patterns of the obtained $CoWO_4$ prepared in different solvents at 150 °C for 12 hours were shown in Fig. 1. Most of the peaks in the XRD patterns of the obtained products (curve a - d) can be assigned to monoclinic $CoWO_4$ (a = 4.6698 Å, b = 5.6873 Å, c = 4.9515 Å and β= 90.0 °, JCPDS Card No. 72-0479). The peaks at 2θ = 15.57 °, 18.99, 23.81, 24.65, 30.63, 31.43, 36.40, 38.52, 41.37, 44.33, 45.79, 48.73, 50.54, 52.02, 54.04, 61.75, 65.05, 68.62 and 71.93 were attributed to the basal planes of (010), (100), (011), (110), (111), (020), (021), (200), (121), (112), (211), (022), (220) , (130), (221), (113), (132), (320) and (-213), respectively. In Fig.1, all of the obtained products from different solvents exhibited nearly the same XRD patterns with sharp and narrow diffraction peaks, which demonstrated that all of the obtained products have high crystal degree and the solvents have little influence on the crystallinity of the products.

In addition, when the reaction time exceeds 12 hours, the XRD patterns of the samples prepared at different reaction time present that the crystalline state of the samples are independent in reaction times, so the selected reaction time is 12 hours on the following studies.

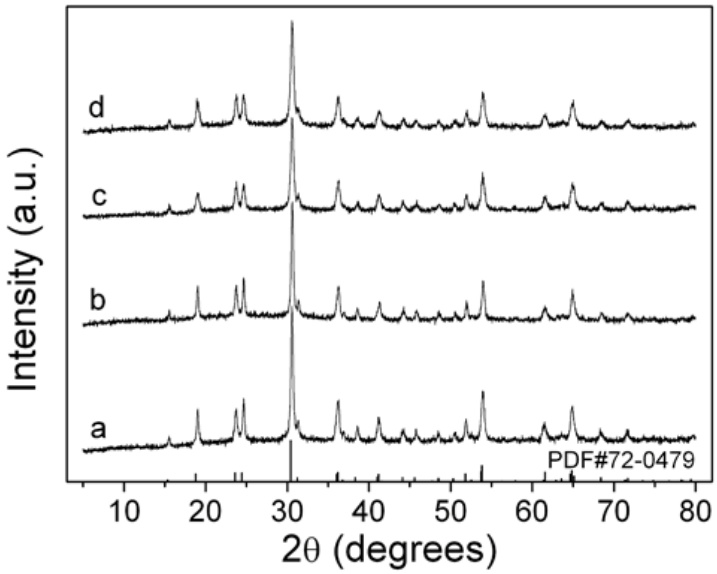

Figure 1. XRD patterns of $CoWO_4$ prepared in different solvents. Curves a to d corresponding DI water, DI water-Et, DI water - Et and DI water-Et-Eg, respectively.

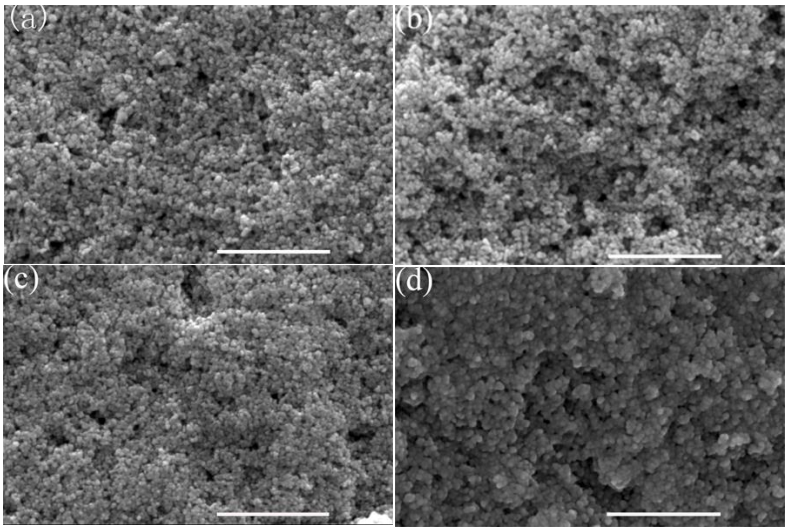

Figure 2. SEM images $CoWO_4$ prepared in different solvents. Curves a to d corresponding DI water, DI water-Et, DI water - Et and DI water-Et-Eg, respectively，the scale bar is 1 μm.

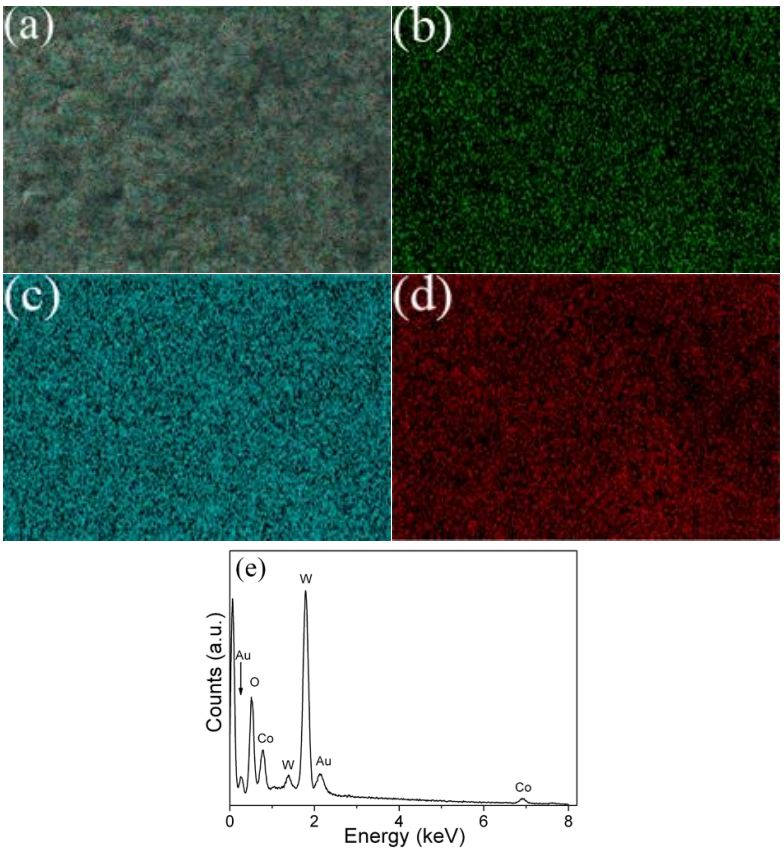

Figure 3. (a) EDS layered image of $CoWO_4$ nanoparticles for elemental analysis. (b−d) Elemental mappings of Co, W, and O, respectively.(e)EDS spectrum of $CoWO_4$ nanoparticles.

Fig. 2 shows the SEM images of obtained $CoWO_4$ prepared in different solvents at 150 °C for 12 hours. It can be observed that the products obtained with DI water, DI water-Et and DI water-Eg present irregular nanoparticles with size of about 15-35 nm, and these nanoparticles have good

dispersion, as depicted in Fig. 2a-c. When the solvent of DI water-Et-Eg was used, the synthesized sample accumulate in a degree with a individual size of around 30 – 60 nm (Fig. 2d).

A detailed composition analysis of the obtained $CoWO_4$ nanoparticles was carried out using EDS elemental mapping. The experimental results show that the EDS results of the products prepared in the above four kinds of solvents have no obvious difference. Fig. 3a presents the EDS layered image of the product prepared in the solvent of DI water-Et. The elemental maps of the constituting elements Co, W and O (Fig. 3b-d) clearly demonstrate a well-defined compositional profile of $CoWO_4$ nanoparticles. From Fig. 3e, only those peaks with the elements of Co, W, O and Au are present in the EDS spectrum, the peaks of Co, W and O are come from the obtained products and the Au peaks arise from the gold sputtered on the sample surface. The contents (*wt*%) of Co, W and O in the product are about 15.0, 15.4 and 48.2, respectively, thereby, the atomic ratio of Co, W and O is 1 : 1.09 : 3.73, which is approximate to the atomic ratio of $CoWO_4$. This result also confirmed that $CoWO_4$ nanoparticles have been successfully synthesized.

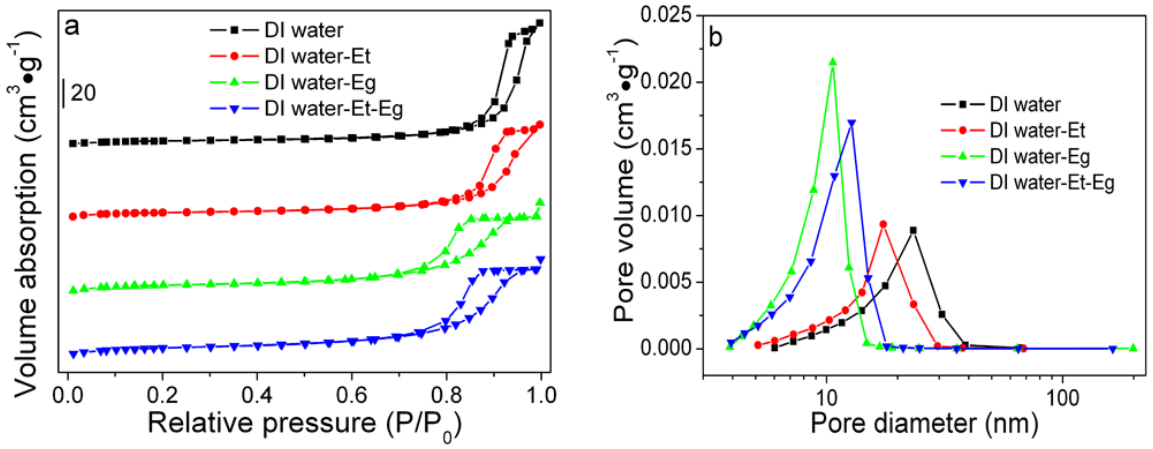

Figure 4. BET isotherms (a) and BJH pore size distribution (b) of $CoWO_4$ prepared in different solvents.

Table 1. The BET surface area and pore properties of $CoWO_4$ prepared in different solvents.

Solvents	BET surface area ($m^2 \cdot g^{-1}$)	Pore range (nm)	Peak pore (nm)
DI water	22.16	6.0-37.7	23.31
DI water-Et	17.96	5.1-29.5	17.39
DI water-Eg	28.04	3.9-16.8	10.63
DI water-Et-Eg	28.24	3.9-18.0	12.77

Fig. 4a shows the nitrogen adsorption/desorption isotherm of the $CoWO_4$ nanoparticles synthesized from different solvents. The mesoporous nature of the products are proved by the irreversible type IV adsorption/desorption isotherm, as shown in curve a to d. The BET surface area of the products obtained in DI-water, DI water-Et, DI water-Eg and DI water-Et-EG are 22.16, 17.96, 28.06 and 28.24 $m^2 \cdot g^{-1}$, respectively. In curve a and b, the similar type H3 hysteresis loops indicate

that the irregular pore structure may be derived from the aggregation of irregular tiny particles. However, when Eg was added to the solvents, the obtained hysteresis loops resembling type H1, as shown in curve c and d, which implies that there are many spherical particle aggregation with uniform size in the as-prepared products. The distinctively different with the change of hysteresis loop types, suggesting the solvents plays a crucial role for the formation of different type of pore structure in the synthesized products. The BJH pore size distribution of the above materials is shown in Fig. 4b. The BET surface area and pore properties of $CoWO_4$ prepared in different solvents were also listed in Table 1. Although the BET surface area of the obtained products are less than the reported literature, the pore size of our products is much high than that of the literature [19], and the larger pores are benefits for the electrolyte ions permeating through the electrode materials, which may result in high *Cs* values. The experimental results clearly revealed that the pore size distribution and peak pore of the product were depended on the applied solvents and gradually decreased in the order of DI water, DI water-Et, DI water-Et-Eg and DI water-Eg. And the effect of the addition of ethylene glycol on the pore size distribution and the location of peak pore of the product was more significant than adding ethanol in DI water.

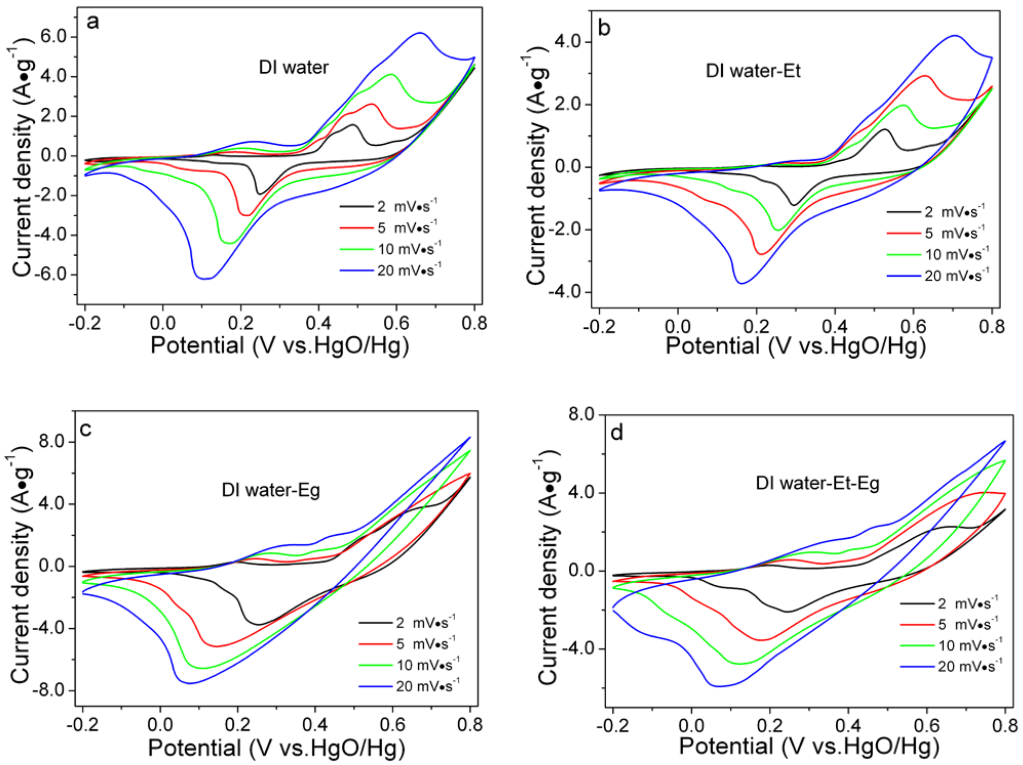

Figure 5. CV curves of $CoWO_4$ prepared in different solvents. Curves a to d corresponding DI water, DI water-Et, DI water - Et and DI water-Et-Eg, respectively.

According to the reported literatures, different solvents do not only result in different homogenization of the reactants in the reaction medium, other parameters in the process of crystal growth such as the amount of individual nucleus formation, the direction preference of the growing

nucleus, and the amalgamation are also largely affected by the solvents [23]. In this research, as the viscosity of the solvent is gradually increased in the order of water, ethanol and ethylene glycol, we speculate that the amalgamation of the products are affected by the viscosity of the solvent, therefore, the pore size distribution and peak position of the pore of the products become narrow and smaller with increasing the viscosity of the solvent, and the further research is underway.

The electrochemical performances of the obtained $CoWO_4$ were firstly evaluated through CV measurements in the potential range of -0.2 to 0.8 V at diverse scan rates, and the electrolyte is 6.0 mol·L^{-1} KOH. As shown in Fig. 5, in the required potential range, all of the products synthesized in the above solvents present redox peaks, the observed redox peaks are due to the charge-transfer kinetics of Co^{2+}/Co^{3+} in the metal tungstate [5]. But the peaks for $CoWO_4$ harvested in DI water or DI water- Et (Fig. 5a and 5b) are more obvious than those obtained in DI water-Et or DI water-Et-Eg (Fig. 5c and 5d), implying that the $CoWO_4$ harvested in DI water or DI water-Et exhibits more easily redox reaction than those obtained in DI water-Et or DI water-Et-Eg. The mainly reason is that the peak pore and pore range of the $CoWO_4$ harvested in DI water or DI water-Et are larger than that of $CoWO_4$ obtained in DI water - Et or DI water-Et-Eg (Table 1), and large pore is in favor of the accessing of electrolyte to inner surface of the materials. The deviation in the shape of the CV curves in Fig. 5c and 5d also proved the low interaction between the electrolyte ions and the electrode. Besides, with the increase of the scan rates, the anodic and the cathodic peaks shift to positive and to negative potentials, respectively. It is worth noting that the peak current density in Fig. 5c and 5d are obviously higher than that in Fig. 5a and 5b, demonstrating the higher specific capacitance (*Cs*) values of $CoWO_4$ obtained in DI water-Et or DI water-Et-Eg.

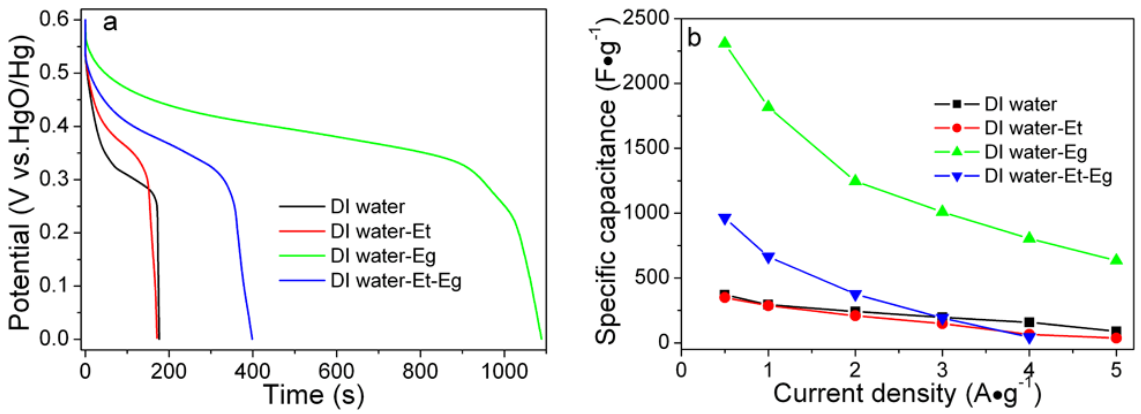

Figure 6. Discharge profiles at a current density of 1.0 A·g^{-1} (a) and specific capacitance values at different discharge current densities (b) of $CoWO_4$ prepared in different solvents.

In order to further explore the performances of the obtained $CoWO_4$ materials, galvanostatic charge–discharge measurements were performed at different constant current densities. Fig. 6a presents the discharge behaviors of $CoWO_4$ materials prepared in different solvents at a current density of 1.0 A·g^{-1}. Apparently, well-plateaus region during the discharge processes was observed, suggesting that the as-prepared $CoWO_4$ materials have excellent pseudocapacitive behaviors. The accurate *Cs* values of the active materials is calculated from the galvanostatic discharge curves based

on the following equation: $C_s = \frac{i \times \Delta t}{\Delta V}$, where i is the discharge current density, Δt is the duration for a full discharge, and ΔV is the voltage change after a full discharge. When the discharge current density is 1.0 $A \cdot g^{-1}$, the calculated *Cs* value of the $CoWO_4$ materials prepared in DI water, DI water-Eg, DI water- Et and DI water-Et-Eg are 294.55, 286.62, 1 817.14 and 664.49 $F \cdot g^{-1}$, respectively. Combining this *Cs* values and the data in Table 1, it can be speculated that the *Cs* values are determined by the surface area and pore distribution of the active materials; and the pore distribution is the major factor , which result in the utilization of the active materials. Fig.6b shows the specific capacitances of $CoWO_4$ materials synthesized in the above solvents under different current densities. Importantly, at the same current density, the specific capacitances of the $CoWO_4$ prepared in the mixed solvent of DI water and ethylene glycol is much larger than that of $CoWO_4$ synthesized in other solvents. This improvement can be attributed to the higher specific surface area and proper pore distribution of the resultant products.

The cyclic stability of the electrode material is very important for practical applications. The above $CoWO_4$ electrodes were employed in charge/discharge test at current density of 1.0 $A \cdot g^{-1}$ up to 1 000 cycles. Fig. 7 shows the profile of capacitance retention with number of cycles. It is clearly observed that all the specific capacitances of the above $CoWO_4$ materials slightly decreased over 1000 cycles, indicating the good cycle performance. Approximately, 92.0% of the specific capacitance was retained after 1000 cycles for $CoWO_4$ materials prepared in DI water-Eg, which was higher than that of $CoWO_4$ prepared in DI water (80.0%), DI water-Et (82.0%) and DI water-Et-Eg (87.4%), respectively. A decrease in specific capacitance can be attributed to dissolution, aggregation, and the volume change occurred in the electrode materials [24].

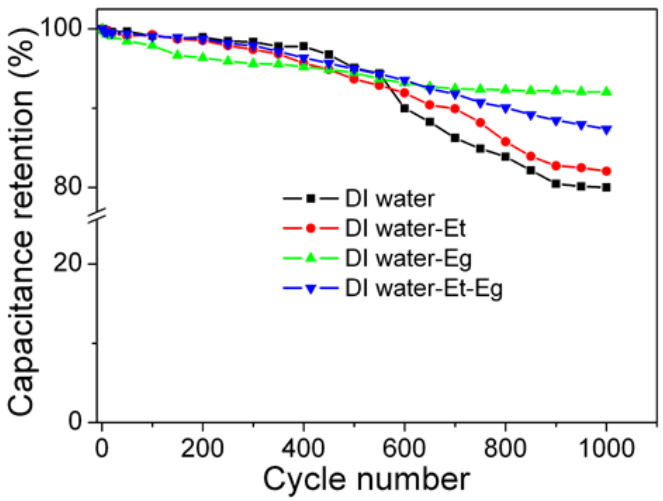

Figure 7. Cycling performance of of $CoWO_4$ prepared in different solvents at the current density of 1.0 $A \cdot g^{-1}$.

Fig. 8 shows the Nyquist plot of the obtained $CoWO_4$ materials at their opening potential with a frequency range from 10^5 to 0.01 Hz in 6.0 $mol \cdot L^{-1}$ KOH aqueous solution, $Z^{/}$ and $Z^{//}$ are the real and imaginary parts of the impedance, respectively. From Fig. 8, it can be observed that the intercepts with

the real axis at the high frequency range of the four electrodes are almost the same, indicating all of the electrodes present nearly equal solution resistance.

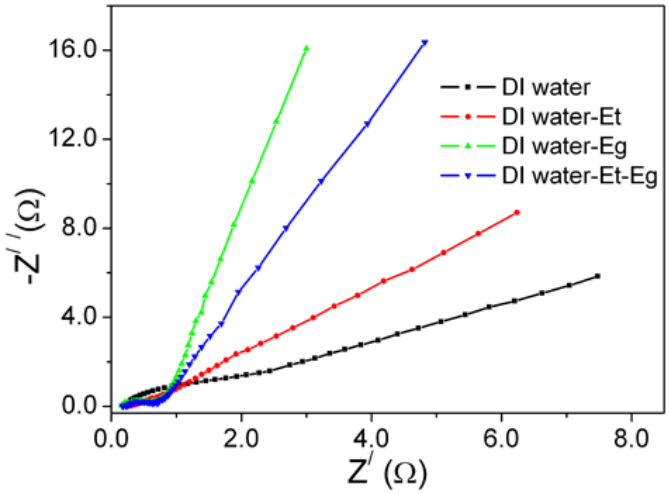

Figure 8. Nyquist plots of $CoWO_4$ prepared in different solvents.

However, the semicircles in the high frequency range are significantly different. The small semicircles diameters of $CoWO_4$ materials prepared in the medium containing ethylene glycol indicated that this materials have low interfacial charge-transfer impedance [25]. It is favorable for electrolyte penetration and fast ion/electron transfer [26]. Besides, the $CoWO_4$ obtained in the mixture of DI water-Eg has the most vertical line in the low frequency range, suggesting that the ion diffusion into the interior of the material would result in greater variations in ion diffusion path lengths and an increased obstruction of ion movement, this result is similar to $NiCo_2S_4$ materials obtained in various solvents [23].

4. CONCLUSIONS

In summary, $CoWO_4$ nanoparticles with different surface area and pore distribution have been successfully fabricated through a facile hydrothermal route by employing different solvents. The pore size distribution and peak pore of the product were depended on the applied solvents, and he surface area and pore distribution of the active material can be easily controlled by adjusting the components of different solvents. Compared to the reported literatures, the obtained $CoWO_4$ products exhibit superior pseudocapacitive performance. In specific, the product synthesized in the mixture of DI water-Eg exhibits a maximum specific capacity of 1 817.14 $F \cdot g^{-1}$ at a current density of 1.0 $A \cdot g^{-1}$, and retains 92.0% of the specific capacitance after 1000 cycles. The high electrochemical performance is attributed to the higher specific surface area and proper pore distribution of the resultant products. This surface area and pore distribution controlled synthesis may provide an alternative strategies for synthesize promising electrode for supercapacitors.

ACKNOWLEDGMENTS
This work was supported by Natural Science Foundation of Jiangsu Province (BK20160425), the Industrial Support Project of Huaian of Jiangsu Province (HAG 2012003), the overseas training project of Jiangsu Province for outstanding young teachers and principals in colleges, the Foundation of Jiangsu Provincial Engineering Laboratory for Advanced Materials of Salt Chemical Industry (SF201401), and the College Natural Science Foundation of Jiangsu Province (13KJB530002).

References

1. C. Liu, F. Li, L.P. Ma and H.M. Cheng, *Adv. Mater.*, 22(2010), E28.
2. S.G. Kandalkara, D.S. Dhawaleb, C.-K. Kima and C.D. Lokhande, *Synthetic Met.*, 160(2010) , 1299.
3. C. Meng, C. Liu, L. Chen, C. Hu and S. Fan, *Nano Lett*., 10(2010), 4025. 4. M. El-Kady, V. Strong, S. Dubin and R. Kaner, *Science*, 335(2012), 1326.
4. C. Yuan, L. Yang, L. Hou, J. Li, Y. Sun, X. Zhang, L. Shen, X. Lu, S. Xiong and X. Lou, *Adv. Funct. Mater.*, 22(2012), 2560.
5. X. Xu, J. Shen, N. Li and M. Ye, *Electrochim. Acta*, 150(2014), 23.
6. L. Feng, Y. Zhu, H. Ding and C. Ni, *J. Power Sources*, 267(2014), 430.
7. M. Winter and R.J. Brodd, *Chem. Rev.*, 104(2004), 4245.
8. B.E. Conway, Electrochemical Supercapacitors: Scientific Fundamentals and Technological Applications, Kluwer Academic, (1999)New York.
9. F. Beguin and E. Frąckowiak, Supercapacitors, Wiley, (2013) Weinheim
10. I.H. Kim and K.B. Kim, *J. Electrochem. Soc.*, 153(2006), A383.
11. S. Muthamizh, R. Suresh, K. Giribabu, R. Manigandan, S.P. Kumar, S. Munusamy, and V. Narayanan, *J. Alloy. Compd.*, 619(2015), 601.
12. X. Xing, Y. Gui , G. Zhang and C. Song, *Electrochim. Acta*, 157(2015), 15.
13. Q. Lu, J.G. Chen and J.Q. Xiao, *Angew. Chem. Int. Ed.*, 52(2013), 1882.
14. C. Ling, L. Zhou and H. Jia, *RSC Adv.*, 4(2014), 24692.
15. H. Jia, J. Stark, L. Zhou, C. Ling, T. Sekito and Z. Markin, *RSC Adv.*, 2(2012), 10874.
16. R. Bharati and R.A. Singh, *J. Mater. Sci.*, 18(1983), 1540.
17. X. Xu, J. Gao, G. Huang, H. Qiu, Z. Wang, J. Wu, Z. Pan and F. Xing, *Electrochim. Acta*, 174 (2015), 837.
18. X. Xu, J. Shen, N. Li and M. Ye, *Electrochim. Acta*, 150(2014), 23.
19. Y. Wang, C. Shen., L. Niu., Z. Sun., F. Ruan.,M. Xu, S. Shan ., C. Li., X. Liu., Y. Gong, *Mater. Chem. Phys.*, 182 (2016), 394.
20. R. D. Kumar and S. Karuppuchamy, *J. Alloy. Compd.*, 674 (2016), 384.
21. J. Zhang, L. D. Sun, J. L. Yin, H. L. Su, C. S. Liao and C. H. Yan, *Chem. Mater.*, 14 (2002), 4172.
22. M. Li, A. Li, H. Xu and L. Feng, *Int.J. Electrochem. Sci.*, 10(2015), 4405.
23. Y. Zhang, M. Ma, J. Yang, C. Sun, H. Su, W Huang and X. Dong, *Nanoscale*, 6(2014), 9824.
24. S. Park and S. Kim, *Electrochim. Acta*, 89 (2013), 516.
25. X. Y. Liu, S. J. Shi, Q. Q. Xiong, L. Li, Y. J. Zhang, H. Tang, C. D. Gu, X. L. Wang and J. P. Tu, *ACS Appl. Mater. Interfaces*, 5 (2013), 8790.
26. G. P. Wang, L. Zhang and J. J. Zhang, *Chem. Soc. Rev.*, 41 (2012), 797.